Materials Research Express

PAPER • OPEN ACCESS

The effect of Ni doping on the electrical and magnetic properties of $Y_{1-x}Ni_xBa_2Cu_3O_{7-\delta}$ delta superconductors

To cite this article: B Hadi-Sichani *et al* 2020 *Mater. Res. Express* **7** 056002

Materials Research Express

PAPER

The effect of Ni doping on the electrical and magnetic properties of $Y_{1-x}Ni_xBa_2Cu_3O_{7-\delta}$ delta superconductors

B Hadi-Sichani, H Shakeripour and H Salamati

Department of Physics, Isfahan University of Technology, Isfahan 84156-83111, Iran

E-mail: hshakeri@iut.ac.ir

Keywords: cuprate superconductors, flux pinning, Ni doping, critical current density

OPEN ACCESS

RECEIVED
4 March 2020

REVISED
4 May 2020

ACCEPTED FOR PUBLICATION
5 May 2020

PUBLISHED
15 May 2020

Abstract

The $Y_{1-x}Ni_xBa_2Cu_3O_{7-\delta}$ superconducting samples with low level of Ni concentration were prepared by the standard solid-state reaction. The AC susceptibility, magnetoresistivity, microstructure and the critical current density, J_c, of samples as a function of temperature, magnetic field and Ni doping are investigated. The AC susceptibility measurements show that the displacement of the peak temperature T_p of the imaginary part of the susceptibility χ'' versus magnetic field was reduced strongly by Ni doping up to an optimum level, which shows the increasing of flux pinning by Ni doping. The J_c of samples was derived from AC susceptibility utilizing the Bean model. It shows an increasing in J_c by Ni doping, at any temperature or magnetic field, consistent with the results of J_c measurements. The magnetoresistance measurements were carried out under magnetic fields up to 1 T and explained by TAFC model. Utilizing this model, the vortex dynamic behaviour and the activation energy U (H) of the compound are investigated. We found that the U (H) increases and the resistive broadening is strongly reduced by Ni doping. The SEM measurements show that the grain sizes are clearly increased and the grain connections are improved by Ni doping. The results of all the observations taken from different measurements are consistent together and indicate the Ni doping has an effective role to improve the intergranular coupling and flux pinning.

1. Introduction

$YBa_2Cu_3O_{7-\delta}$ (Y-123), the first discovered superconductor with critical transition temperature, T_c, higher than the boiling temperature of liquid nitrogen, has grown widely in industry and applications [1, 2] due to its high T_c. However, due to weak flux pinning, this high temperature superconducting (HTSC) material has limitations [3–5]. After the discovery of HTSC, various efforts have been carried out to increase the value of the critical current density, J_c, in these materials. It is well known that, by eliminating flux motion, the J_c increases. Many experimental efforts have been made to study the relationship between the dissipative flux motion and the flux pinning mechanisms. They have proposed some reasons such as flux line melting [6, 7], thermally activated phase slip (TAPS) [8], flux flow [9] and thermally activated flux creep (TAFC) [10] for vortex dynamics. On the other hand, the complex vortex dynamics, poor flux pinning and weak intergrain links are major limiting factors. Substitutions like oxides [11–13], nanoparticles and carbon nanotubes (CNT) [14, 15] and metals [16–21] in cuprates have enhanced their prospectus for promising applications. It is found that Y in Y-123 system could be replaced by almost all the rare earth (RE) (Gd, Ho, Nb etc) elements [16–18]. Doping of Gd [16], Ho [17], Nb [18] and composites with NiO [11], graphene [14], Au [19], graphene oxide [22] have resulted in the enhancement of flux pinning. Also, substitution of nonmagnetic and magnetic elements such as Zn and Ni, for Cu site in Y-123, modify the flux pinning mechanisms in the compound then led to J_c increasing. However, to have high J_c through these kind of doping it needs a large amount of doping to add which led to strong suppression of T_c. It is believed that these impurities sit on the Cu of the CuO_2 plane and reduce T_c strongly. In spite of many efforts to reduce the dissipative flux motion and to increase J_c in HTSC however no clear way has emerged yet.

Here, we have investigated a possible way to improve flux pinning in Y-123 by substitution of *very low* concentrations of *magnetic* Ni element *for the Y site*. We study the magnetic susceptibility, magnetoresistivity, microstructure and the critical current density of $Y_{1-x}Ni_xBa_2Cu_3O_{7-\delta}$ compound as a function of temperature, magnetic field and Ni doping to investigate the vortex dynamic behaviour, pinning forces and intergranular coupling in these HTSC materials. We found that by substitution of a *low* amount of Ni *for* Y *atom* (0.4%), the flux pinning, the grains coupling and the critical current density increase strongly, which is an efficient way for the technological application.

2. Experimental

The $Y_{1-x}Ni_xBa_2Cu_3O_{7-\delta}$ samples with $x = 0.000, 0.002, 0.004, 0.006, 0.008, 0.010$ and 0.020 have been prepared by a solid-state reaction method. High purity powders of Y_2O_3, $BaCO_3$, CuO and NiO were mixed according to exact stoichiometric amounts. The aforesaid mixture was thoroughly ground and calcined in air at 840 °C for 24 h and then cooled down slowly to room temperature. The calcination with intermediate grinding was repeated twice. After final calcination the powder product was pressed into pellets under a pressure of 40 bar. In order to obtain the fully oxygenated samples, the pellets were sintered in the presence of pure oxygen flow at 950 °C for 24 h [23]. The samples have the rectangular shape with dimension of $10 \times 2 \times 1.3\ mm^3$.

The powder x-ray diffraction of the samples was taken using CuK_α radiation. The Rietveld analysis of XRD of all samples was performed using Fullprof program. The results showed that all the samples are crystallized in single phase, having an orthorhombic structure with a space group *Pmmm* and no detectable impurity phases [24].

The electrical resistivity and magnetoresistance measurements were carried out by a DC four-probe method over the temperature range 20–300 K. The applied magnetic field was from 0 up to 1 T. The applied current was 10 mA. The AC magnetic susceptibility measurements were performed using a Lake Shore AC Susceptometer Model 7000. The AC magnetic field, H_{AC}, was in the range 0.8–800 A m^{-1} with a frequency of 333 Hz, in the temperature range 77–100 K. The transport critical current density was measured using the four-probe technique at 77 K. The SEM images of the samples were taken using a Philips XL 30 Scanning Electron Microscope.

3. Results and discussion

3.1. AC suseptibilty

AC magnetic susceptibility is made of two parts (χ', χ''), real part, χ', and imaginary part, χ''. The real part, χ', is a measurement of the magnetic shielding generated by supercurrents or a measure of flux penetration into the sample, while the imaginary part, χ'', is a measure of the energy dissipation and the power losses in the material. Figure 1 shows the temperature dependency of the real, χ', and imaginary, χ'', parts of AC susceptibility for all $Y_{1-x}Ni_xBa_2Cu_3O_{7-\delta}$ samples at different AC field amplitudes, $H_{AC} = 0.8$, 200, 400 and 800 A m^{-1}. By lowering the temperature, the real part shows a transition from normal state to the diamagnetic superconducting phase, at a transition temperature consistent with what is reported in the literatures. Also, looking at the imaginary parts, it can be seen from the curves that the peak of χ'' shifts to lower temperatures and also broadens when the magnetic field increases (see figures 1(a) and (b), for example). The strength of the shift and broadening of χ'' peak as a function of field amplitude is proportional to the strength of the vortex pinning force in the compound and is due to field penetration and the hysteretic losses for the motion of Abrikosov vortices between the grains [25].

Moreover, the shift and the broadening of the peak is reduced, by Ni doping up to the optimum dopant, $x = 0.004$, figure 1(c). Figure 1(c) shows the strength of the shift of imaginary peak in $Y_{0.996}Ni_{0.004}Ba_2Cu_3O_{7-\delta}$ sample is too small and much less than in all other samples with different Ni-dopant concentrations. By increasing of Ni doping above 0.4%, the displacement of the peak and the broadening increase (see figure 1(e) for $x = 0.02$ sample).

In figure 1(f), the variations of the imaginary peak temperature, T_p, as a function of AC magnetic field amplitude H_{AC}, for all samples, have been plotted. T_p is the temperature where the imaginary peak appears, at each applied field amplitude H_{AC}; See arrows in figure 1(a). For example, for Y-123 sample, $T_p \sim 90.3$ K at $H_{AC} = 0.8$ A m^{-1}. Each plot for each sample in figure 1(f) shows that by increasing field amplitude, the T_p is shifted to lower temperatures, due to the flux motion. Also, it shows that the rate of the T_p shift as a function of field amplitude is reduced by Ni doping, up to the optimum level ($x \approx 0.004$); for $x = 0.004$ sample, all imaginary peaks, related to each applied field, appear at one temperature point and show nearly one T_p, figures 1(c) and (f). These observations suggest that the pinning force and the intergranular coupling have improved by Ni doping which would lead to an increase in the critical current density of the sample too (see below).

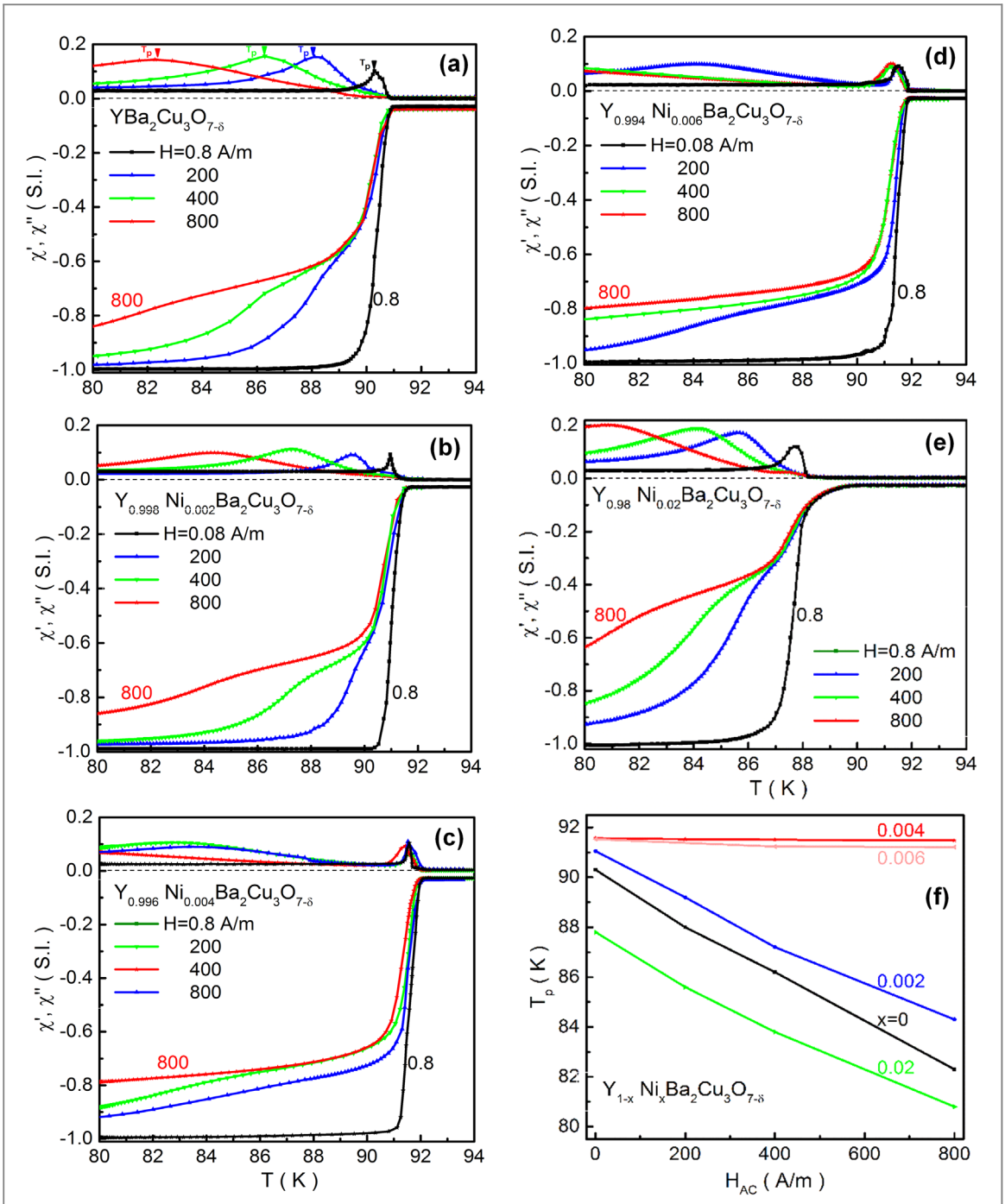

Figure 1. Temperature dependence of the AC magnetic susceptibility of $Y_{1-x}Ni_xBa_2Cu_3O_{7-\delta}$ samples with (a) x = 0, (b) 0.002, (c) 0.004, (d) 0.006 and (e) 0.02, in various AC field amplitudes H_{AC} = 0.8 , 200, 400, 800 A m^{-1}. The position of the appeared imaginary peak at each field is called T_p, shown by arrows in (a). It is clearly seen that the T_p is shifted to low temaperatures and the peak becomes broaden by increasing field amplitude. Also, the shift and the boadening of the peak is reduced, by Ni doping up to the optimum dopant, x = 0.004 (c). The degree of shift of the peak is lowest for x = 0.004 sample (optimaly doped sample (c)). Above the optimal dopant, the shift and the broadening increase (d), (e). (f) Field amplitude dependence H_{AC} of the peak temperature T_p in $Y_{1-x}Ni_xBa_2Cu_3O_{7-\delta}$ (x = 0, 0.002, 0.004, 0.006 , 0.002). For each sample, the T_p is reduced by increasing of H_{AC}. By incresaing of Ni doping up to x = 0.004, the rate of T_p reduction versus H_{AC} becomes strongly weak (see red data for optimally doped sample x = 0.004; T_p is nearly field independent (f)). The amount of the T_p shift as a function of the applied field amplitude is proportional to the strength of the pinning force in the sample.

The measurement of AC susceptibility is widely used as a powerful method for characterization of the intergrain behaviours and critical current density concerning the weak links [26] in HTSC. It gives useful information on the vortex pinning force, magnetic losses and fluxon dynamics [25, 27]. There are some models for interpreting AC susceptibility data, such as Clem [28], Kim [29], single-loop (or surface-sheath) [30, 31], Peterson and Ekin [32, 33], and the critical state Bean model [27, 34, 35]. The latter model is most used for estimating the critical current in HTSC [36].

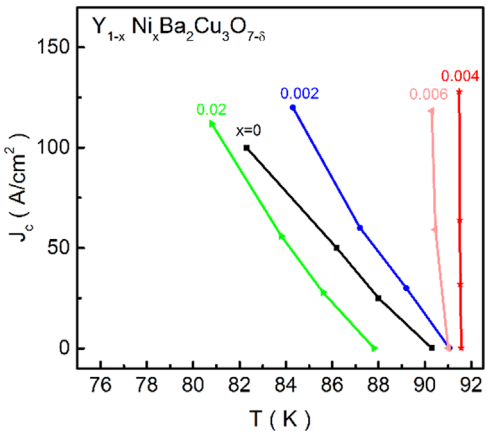

Figure 2. Temperature dependence of the intergranular critical current density Jc of $Y_{1-x}Ni_xBa_2Cu_3O_{7-\delta}$ samples. Jc is derived from figures 1(a)–(e) and using the Bean model and utilizing equation (1). By considering of a vertical guide line at each temperature point, it is clearly seen by increasing of Ni concentration up to x = 0.004, the Jc increases and the 0.4% doped sample has the highest Jc among all samples. Above the optimally doped, Jc reduces (see x = 0.02 sample).

In order to analyse the AC susceptibility data and to obtain the temperature dependence of the intergranular critical current density, we utilize the Bean model, for bar-shaped samples [35]:

$$J_c = \frac{H_{AC}}{(ab)^{\frac{1}{2}}} \tag{1}$$

where 2a × 2b, a < b, is the cross section of the rectangular bar-shaped sample, H_{AC} is the amplitude of the applied AC field and J_c is the intergranular critical current density at T_p. The Bean model use the observed values of χ' and χ'', at T_p, to determine the intergranular shielding currents. The theoretical treatment of the model involves discussion of the Lorentz force on vortices that is proportionate to the product of the current and the local field at that point [27].

Figure 2 shows the temperature variation of the calculated J_c by equation (1), for all the samples. It is obvious that the $Y_{0.996}Ni_{0.004}Ba_2Cu_3O_{7-\delta}$ sample has higher J_c than that of other samples (at each temperature point); see red data for x = 0.004 sample in figure 2. For example, J_c is 50 A cm^{-2} at T = 86 K for pure sample (black data for x = 0.0 in figure 2). However, at the same temperature, it would be too large for 0.4% Ni-doped sample (red data in figure 2). Xu *et al* [37] and Zhang *et al* [38] in $GdBa_2Cu_3O_{7-\delta}$/magnetic powder, Lau *et al* [39] in BiSCCO/nanorod Fe_2O_3 composite and El-Aziz *et al* [40] in YBCO/NiO composite were reported an increasing in Jc and in the strength of pinning.

3.2. The resistivity

Another prominent method to study HTSC is to investigate the electrical resistivity transition under applied magnetic field. The resistivity transition, due to granular nature of cuprates [13], is made of two parts [41, 42]. The first part, near the onset of superconductivity, is due to superconductivity in grains. Another broadened part is observed along the tail of transition which is attributed to the coupling between grains. This resistive broadening under magnetic field can be interpreted by some different models, such as flux line melting [6] and TAPS [8], TAFC [10], flux entanglement [43]. TAPS model was described by the Ambegaokar and Halperin [8] theory. It was used to describe the observed broadening in the resistance curves of granular YBCO [44, 45], BSCCO [46], GdPrCa-123 [23] and $TmBa_{2-x}Pr_xCu_3O_{7-\delta}$ [47]. Most authors [48, 49] pointed out that the TAFC model can describe the broadening of superconducting transition. Thermally activated flux creep model explains the percolation nature between grains and the broadening behaviour in the low-resistance region near T_{c0} ($\rho = 0$) (when the pinning force dominates, $U \gg k_BT$) [41, 42, 50], while the flux flow regime appears near the onset transition temperature, where $U \approx k_BT$. According to TAFC model, the resistivity data in the broadening tail part can be described by the Arrhenius relation (see below).

The electrical resistivity of samples was measured versus temperature and under applied DC magnetic field. The normal state resistivity is unaffected by the applied magnetic field. In fact, magnetic fields up to 1 T are too weak to affect the normal state of YBCO.

Figure 3(a) shows $\rho(T)$ of $Y_{0.996}Ni_{0.004}Ba_2Cu_3O_{7-\delta}$ sample, for instance, under H = 0, 0.3, 0.6 and 1 T. By application of magnetic field a broadening is appeared in $\rho(T)$ at low temperatures where $\rho(T)$ goes to zero. This broadening is strong in pure sample and decreases with Ni doping up to the optimal dopant [51]. The smallest broadening is observed in the optimally doped sample (x = 0.004) (figure 3(a)).

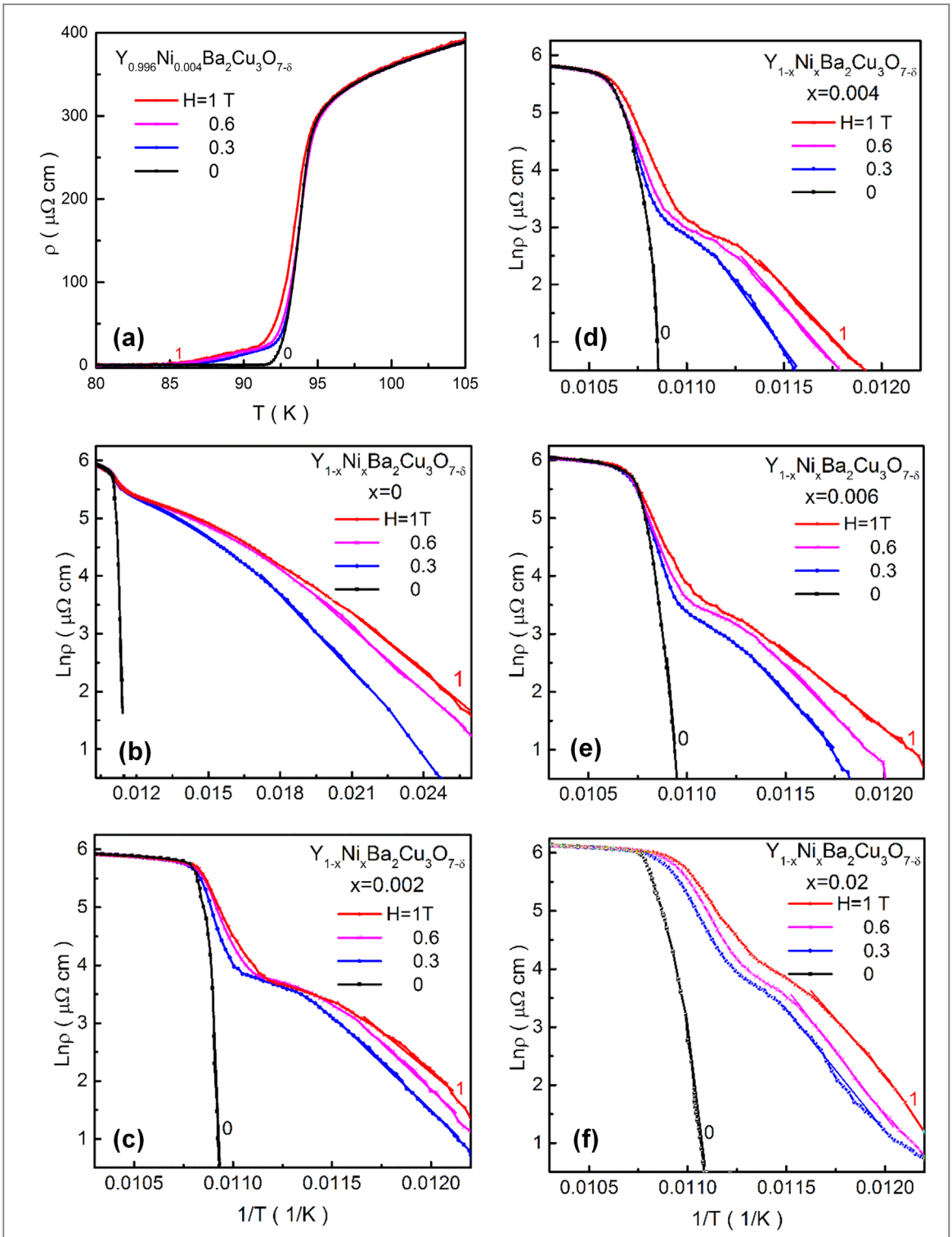

Figure 3. (a) The electrical resistivity versus temperature at various applied magnetic fields: H = 0, 0.3, 0.6 and 1 T, in $Y_{0.996}Ni_{0.004}Ba_2Cu_3O_{7-\delta}$ sample. By increasing magnetic field, a resistive broadening is appeared at low temperatures near T_c ($\rho = 0$). This broadening is smallest in x = 0.004 optimally doped sample [51]. Fitting of the low temperature broadening part within TAFC model, shown in (b)–(f), give good information about the vortex dynamic behaviour in the compound. (b)–(f) The logarithm of resistivity versus $1/T$ is plotted (Arrhenius plot), for $Y_{1-x}Ni_xBa_2Cu_3O_{7-\delta}$ samples with x = 0, 0.002, 0.004, 0.006, 0.002. The slope of the linear fitting part, shown by solid lines on the data, is proportional to the activation energy of vortices (see equation (2)).

The broadening of superconducting transition under applied magnetic field can be analysed in terms of activation energy of vortices, according to Arrhenius equation [52]:

$$\rho(T, H) = \rho_0 \exp\left(-\frac{U(H, T)}{Tk_B}\right) \quad (2)$$

Table 1. The derived activation energy U (H) using TAFC model applied on the resistivity measurements at magnetic fields μ_0 H = 0.1, 0.3, 0.6 and 1 T in $Y_{1-x}Ni_xBa_2Cu_3O_{7-\delta}$ samples with x = 0, 0.002, 0.004, 0.006, 0.02. J_c is measured at 77 K (called $J_{c\ measu}$).

$Y_{1-x}Ni_x$-123	U (0.1 T) meV	U (0.3 T) meV	U (0.6 T) meV	U (1 T) meV	$J_{c\ measu}$ (77 K) A cm^{-2}
x = 0.000	668	45.6	35.4	30	100
0.002	2620	149.8	221.5	180	300
0.004	2660	403.6	329.7	300.8	400
0.006	2536	317.3	293.1	229.6	
0.020	1634	369.8	315.2	267.3	180

where ρ_0 is a field independent factor, k_B is the Boltzmann constant and U is the activation energy. The resistive broadening in the Arrhenius plot was explained first by Palstra *et al* by considering dissipative flux motion within the flux creep model [52]. The activation energy at different fields is extracted using standard technique by plotting $\ln\rho$ as a function of $1/T$, see figures 3(b)–(f). The U values are extracted by a fitting procedure within a temperature region where $\ln\rho$ versus $1/T$ shows nearly a linear behaviour, which is shown by the solid lines in figures 3(b) to (f). Solid lines are the results of linear regression analysis and the slope is proportional to the magnetic field dependence of the activation energy, U (H). The extracted U (H) for $Y_{1-x}Ni_xBa_2Cu_3O_{7-\delta}$ (x = 0.00, 0.002, 0.004, 0.006, 0.02) samples is shown in table 1.

Table 1 indicates two points. First, the activation energy, U (H), is larger for all Ni-doped samples, in each applied magnetic field, compared to pure YBCO. Also, it is largest for the sample with x = 0.004, nearly 2660 meV at H = 0 T, four times larger than of the pure sample (U (0) = 668 meV). It is interesting that in other applied magnetic fields the activation energy in the x = 0.004 sample is 10 times larger compare to the pure sample ones (for example, at H = 1 T, U (H) is 30 and 300.8 meV for pure and x = 0.004 samples, respectively, see table 1). This means the flux pining gets stronger with Ni doping up to the optimum doping (x = 0.004 sample). The value of U (H) has been reported nearly 300 meV to 100 meV under H = 0.3 to 4.5 kG in Gd123 [53], 350 meV to 200 meV under H = 0.3 to 4.5 kG in $GdBa_2Cu_{2.95}Ru_{0.05}O_{7-\delta}$ [53], 400 meV to 100 meV under H = 0 to 1 T in YBCO + 4%BZO [13] and 2400 meV to 400 meV under H = 0 to 1 T in YBCO +%15Ag [54].

Second, looking at the magnetic field dependence of the activation energy, U (H) drops by increasing of H (table 1). The variation of pinning energy versus magnetic field can be represented with a power law relation:

$$U(H) \sim H^{-\beta} \tag{3}$$

where the β power is a constant. It seems the β value depends on the different type of defects and weak links in each compound [55]. As a result, we obtained β = 0.35, 0.26, 0.24, 0.25 and 0.26 for Y-123, $Y_{0.0998}Ni_{0.002}$-123, $Y_{0.996}Ni_{0.004}$-123, $Y_{0.994}Ni_{0.006}$-123 and $Y_{0.98}Ni_{0.02}$-123, respectively. The power law dependency of U (H) has also been reported by others. Some authors have shown the value of β to be 0.5 in Y123 [44], 0.6 in the granular composite of Y123/Y211 [45], 0.36 in Gd123 [23], 0.35 in GdPrCa123 [23], 0.26 in $Gd_{0.85}Ca_{0.15}$123 [23], 0.5 in GdBCO thin film [56] and 0.60 in Y358 [57].

3.3. Critical current density

The critical current density of the samples was measured at liquid nitrogen temperature, 77 K (called $J_{c\ measu}$). Figure 4 shows potential difference as a function of current density, V–J, curves for samples with x = 0.00, 0.002, 0.004, 0.01 and 0.02. J_c of the samples has been obtained by the extrapolation of the linear part of the curves, where the linear extrapolation cut the horizontal axis; see dashed line on the top of x = 0.004 data in figure 4(a), for example. Figure 4(a) shows that the J_c increases by Ni doping up to the optimum doping. Then, by over-doping, the J_c reduces, figure 4(b). The measured J_c values are summarized in table 1. A more detailed examination of table 1 tells us that the J_c and U (H) increase by Ni doping up to x = 0.004, which may be attributed to the enhancement in the inter-grain connectivity. The maximum J_c of 400 A cm^{-2} was obtained in the optimally doped sample at 77 K (figure 4(a)), which is consistent with the derived J_c by Bean model (from the susceptibility measurements).

3.4. The SEM measurements

The scanning electron microscopic (SEM) images of samples with x = 0.00, 0.004, 0.02 are shown in figures 5(a)–(c). It is clearly seen that the optimally doped x = 0.004 sample has better surface texture than pure

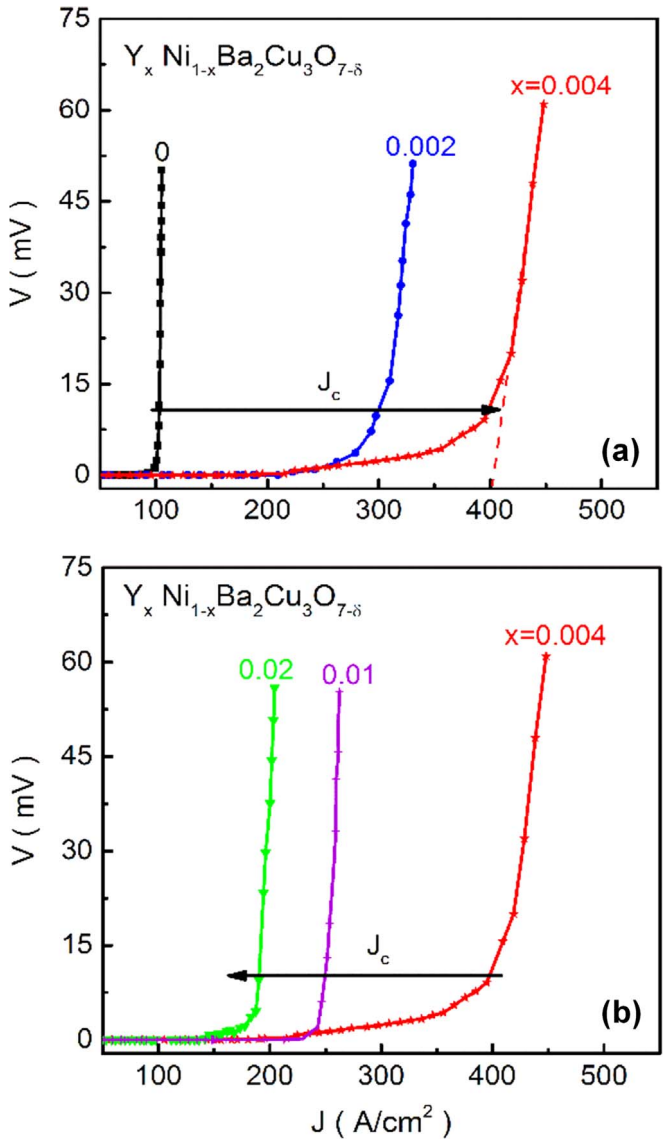

Figure 4. Measured potential difference as a function of current density (Voltage–J) curves for $Y_{1-x}Ni_xBa_2Cu_3O_{7-\delta}$ samples with (a) $x = 0, 0.002, 0.004$ and (b) $x = 0.004, 0.01$ and 0.02. J_c of each sample is where the extrapolation of the linear part of the V-J curve, cut the horizontal axis; see dashed line on the top of $x = 0.004$ data in (a). (a) By increasing Ni dopant to the optimum amount $x = 0.004$, J_c increases. (b) By further doping, J_c reduces. However, all Ni-doped samples have higher J_c than that of the pure sample.

sample and porosity level decreased strongly by Ni doping; see figures 5(b) and (c). The grains with different sizes are distributed in the samples. From figure 5, it is observed that the grain size increases by Ni doping too. Increasing the size of grains is one of the effective ways to minimize the grain boundary area and increase the coupling of superconducting grains and flux pinning. The observation of maximum grain size for 0.4% Ni-doped sample, around 11 μm, (figure 5(b)), is consistent with the observed maximum activation energy (table 1), and the maximum measured and estimated J_c (figures 2 and 4) for this optimally doped sample. Increasing of the grain size by Ni doping may be related to increasing of the unit cell volume by doping, where the optimally doped sample has the highest unit cell volume, as was reported in [24].

Furthermore, figure 5(c) shows that in $x = 0.02$ sample, the inter-grain connectivity is good (this also can be confirmed and consistent with no observation of any extra kink or shoulder in susceptibility measurements of the same sample at low temperatures, see figure 1(e) at 0.8 A m^{-1}). However, it has lower J_c compare to $x = 0.004$ sample. It seems the main key to increase J_c in 0.004 sample is the flux pinning by the doping. This increasing would have an optimum regarding to the doping. To note, in the literatures it has been also reported that the J_c is proportional to the inverse of the gain size; the smaller grains would lead to higher J_c. In this view, although, the $x = 0.02$ sample has smaller grain size compare to $x = 0.004$ one, but has lower J_c. This also confirms the main key of the flux pinning by the doping.

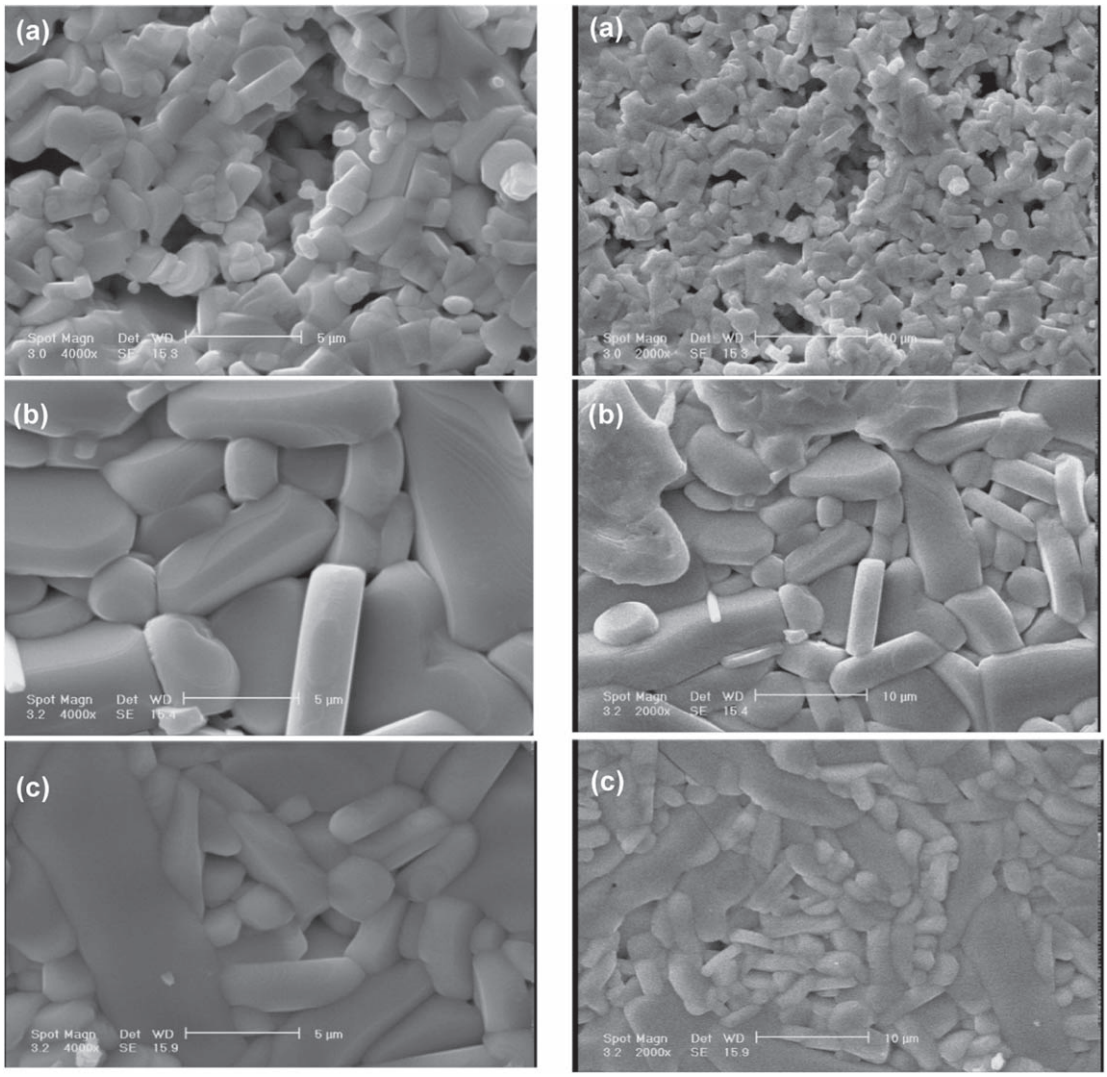

Figure 5. SEM micrographs (scanning electron microscope) of $Y_{1-x}Ni_xBa_2Cu_3O_{7-\delta}$ samples with (a) $x = 0$, (b) 0.004, and (c) 0.02. It is seen that by Ni doping, the grain size is increased strongly and the optimally doped sample, $x = 0.004$ (b), has the largest grain size, around 11 μm. Also, porosity is reduced by Ni doping and grains coupling increased. The micrographs are shown in (Left) 5 μm and (Right) 10 μm resolutions.

4. Conclusion

In conclusion, we have investigated the microstructural and the flux dynamic behavior in superconducting $Y_{1-x}Ni_xBa_2Cu_3O_{7-\delta}$ samples, through SEM, AC magnetic susceptibility, magnetoresistivity and the critical current density measurements. We have studied the variations of vortex pinning, grains coupling and the J_c as a function of Ni substitution *for* Y *atom*. We observe an increase in the pinning force and in the grains coupling by Ni doping up to the optimum doping 0.4%, through susceptibility measurements. The temperature dependence of the AC susceptibility has been analyzed by the Bean model and the variation of the J_c versus temperature and doping was derived. It indicates that the intergranular critical current density increases with Ni doping, which is consistent with the results of J_c measurements. The magnetoresistance measurements have been studied within TAFC model. The results of $\rho(T, H)$ show the magnetic Ni element doping has a beneficial effect on the intergranular coupling and the activation energy strongly. The SEM analysis shows the grain size and the grains connectivity were improved by Ni doping, consistent with the obtained results from other measurements.

We suggest that a small amount of Ni (0.4%) doping for Y atom in Y-123 compound could improve the electrical properties of these materials for their applications. The present study investigates the response of the critical current density of cuprates to the substitution of *magnetic impurity* with *very low* concentrations and *for the* Y *atom*.

Acknowledgments

The assistance of S Hosseini and Kh Rahmani is acknowleged. We also thank Professors F Davar, P Kameli and H Ahmadvand for insightful discussions.

ORCID iDs

H Shakeripour https://orcid.org/0000-0002-3754-9713

References

[1] Hubmayr J 2009 Bolometric detectors for EBEX: a balloon-borne cosmic microwave background polarimeter *PhD Thesis* University of Minnesota
[2] Jiasu W *et al* 1999 A scheme of Maglev vehicle using high T_c bulk superconducters *IEEE Trans. Appl. Supercond.* **9** 904
[3] Blatter G, Feigel'man M V, Geshkenbein V B, Larkin A I and Vinokur V M 1994 Vortices in high-temperature superconductors *Rev. Mod. Phys.* **66** 1125
[4] Ekin J W *et al* 1987 Evidence for weak link and anisotropy limitations on the transport critical current in bulk polycrystalline $Y_1Ba_2Cu_3O_x$ *J. Appl. Phys.* **62** 4821
[5] Obaidat I M, Goeckner H P and Kouvel J S 1997 Vortex pinning in a rotated $YBa_2Cu_3O_{7-\delta}$ crystal *Physica* C **291** 8
[6] Gammel P L, Schneemeyer L F, Wasczak J V and Bishop D J 1988 Evidence from mechanical measurements for flux-lattice melting in single-crystal $YBa_2Cu_3O_7$ and $Bi_{2.2}Sr_2Ca_{0.8}Cu_2O_8$ *Phys. Rev. Lett.* **61** 1666
[7] Nelson D R 1988 Vortex entanglement in high-T_c superconductors *Phys. Rev. Lett.* **60** 1973
[8] Ambegaokar V and Halperin B I 1969 Voltage due to thermal noise in the dc Josephson effect *Phys. Rev. Lett.* **22** 1364
[9] Kim Y B, hempstead C F and Strnad A R 1965 Flux-flow resistance in type-II superconductors *Phys. Rev.* **139** A1163
[10] Anderson P W 1962 Theory of flux creep in hard superconductors *Phys. Rev. Lett.* **9** 309
[11] Zhao Y, Cheng C H and Wang J S 2004 Flux pinning by NiO-induced nano-pinning centres in melt-textured YBCO superconductor *Supercond. Sci. Technol.* **18** S43
[12] Campbell T A, Haugan T J, Maartense I, Murphy J and Barnes P N 2005 Flux pinning effects of Y_2O_3 nanoparticulate dispersions in multilayered YBCO thin films *Physica* C **423** 1
[13] Malik B A, Asokan K, Ganesan V, Singh D and Malik M A 2016 The magnetoresistance of YBCO/BZO composite superconductors *Physica C: Superconductivity and its Applications* **531** 85
[14] Wei K, Ing K, Hamdan M S, Radiman S and Abd-Shukor R 2018 AC susceptibility and superconducting properties of graphene added $YBa_2Cu_3O_{7-d}$ *J. Supercond. Novel Magn.* **31** 1
[15] Dadras S, Liu Y, Chai Y S, Daadmehr V and Kim K H 2009 Increase of critical current density with doping carbon nano-tubes in $YBa_2Cu_3O_{7-\delta}$ *Physica* C **469** 55
[16] Feng Y, Zhou L, Wen J G, Koshizuka N, Sulpice A, Tholence J L, Vallier J C and Monceau P 1998 Fishtail effect, magnetic properties and critical current density of Gd-added PMP YBCO *Physica* C **297** 75
[17] Feng Y, Pradhan A K, Zhao Y, Wu Y, Koshizuka N and Zhou L 2001 Improved flux pinning in $Y_xHo_{1-x}Ba_2Cu_3O_y$ fabricated by powder melting process *Supercond. Sci. Technol.* **14** 224
[18] Salluzzo M, Cassinese A, De Luca G M, Gambardella A, Prigiobbo A and Vaglio R 2004 Transport properties of $Nd_{1.2}Ba_{1.8}Cu_3O_Z$ ultrathin films by field-effect doping *Phys. Rev.* B **70** 214528
[19] Lambert C, Debierre J-M, Albinet G and Marfaing J 1999 Temperature dependence of the resistivity in Au—$YBa_2Cu_3O_x$ sintered composites *Philos. Mag.* B **79** 1029
[20] Mirshamsi S *et al* 2010 Superconducting properties of $Y_{1-x}Tb_xBa_2Cu_3O_{7-\delta}$ and $Y_{1-x}Tb_xSr_2Cu_{2.7}Mo_{0.3}O_{7-\delta}$ *Mod. Phys. Lett.* B **24** 419
[21] Soylu N, Yahsi C C, Altintas S P, Nezir S and Terzioglu C 2013 The structural and electrical study of Lu-doped YBCO system *J. Supercond. Novel Magn.* **26** 1945
[22] Shoushtari M Z *et al* 2018 Study of $YBa_2Cu_3O_{7-\delta}$ superconductor/graphene oxide composite *J. Supercond. Novel Magn.* **31** 1
[23] Shakeripour H and Akhavan M 2001 Thermally activated phase-slip in high-temperature cuprates *Supercond. Sci. Tech.* **14** 234
[24] Hadi-Sichani B, Shakeripour H and Salamati H 2018 Structural investigation of $Y_{1-x}Ni_xBa_2Cu_3O_{7-\delta}$ superconductor *Physica C: Superconductivity and its Applications* **550** 92
[25] LeBlanc D and LeBlanc M A R 1992 AC-loss valley in type-II superconductors *Phys. Rev.* B **45** 5443
[26] Li X F, Grivel J C, Abeahamsen A B and Andersen N H 2012 Critical current density measurement of thin films by AC susceptibility based on the penetration parameter *Physica* C **477** 6
[27] Murphy S D, Renouard K, Crittenden R and Bhagat S M 1989 AC susceptibility of sintered high T_c superconductors—Bean's model and shielding current *Solid State Commun.* **69** 367
[28] Clem J R 1988 Granular and superconducting-glass properties of the high-temperature superconductors *Physica* C **153** 50
[29] Kim Y B, Hempstead C F and Strnad A R 1962 Critical persistent currents in hard superconductors *Phys. Rev. Lett.* **9** 306
[30] Rollins R W and Silcox J 1967 Nature of the ac transition in the superconducting surface sheath in Pb-2% In *Phys. Rev.* **155** 404
[31] Ishida T and Mazaki H 1981 Superconducting transition of multiconnected Josephson network *J. Appl. Phys.* **52** 6798
[32] Peterson R L and Ekin J W 1988 Josephson-junction model of critical current in granular $YBa_2Cu_3O_{7-\delta}$ superconductors *Phys. Rev.* B **37** 9848
[33] Peterson R L and Ekin J W 1989 Airy pattern, weak-link modeling of critical currents in high-T_c superconductors *Physica* C **157** 325
[34] Kumar G R and Chaddah P 1989 Extension of Bean's model for high-T_c superconductors *Phys. Rev.* B **39** 4704
[35] Bean C P 1962 Magnetization of hard sperconductors *Phys. Rev. Lett.* **8** 250
Bean C P 1964 Magnetization of high-field superconductors *Rev. Mod. Phys.* **36** 31
[36] Kameli P, Salamati H and Abdolhosseini I 2008 AC susceptibility study of $Bi_{1.66}Pb_{0.34}Sr_2Ca_{2-x}Mg_xCu_3O_y$ ($x = 0, 0.2$ and 0.4) superconductor systems *J. Alloys and Compounds* **458** 61
[37] Xu Y, Izumi M, Zhang Y F and Kimura Y 2009 Enhancement of critical current density in Gd123 bulk superconductor doped with magnetic powder *Physica* C **469** 1215

[38] Zhang Y, Izumi M, Xu Y, Gao T and Kimura Y 2010 Enhanced performance in bulk superconductor $GdBa_2Cu_3O_7$ with additions of-Fe_2O_3 particles *J. Phys.: Conference Series* **234** 012052
[39] Lau K T, Yahya S Y and Abd-Shukor R 2006 Enhanced flux pinning in Ag-sheathed Bi(Pb)–Sr–Ca–Cu–O superconductors tapes with addition of magnetic nanorod γ-Fe_2O_3 *J. Appl. Phys.* **99** 123904
[40] El-Aziz A M A, Afifi H A, Hager I Z, Abdel Aal N S and Naqib S H Structural, electrical, magnetic, and flux pinning properties of YBCO/Ni superconducting composites: analyses and possible explanations arXiv:1808.03740
[41] Mohammed N H, Abou-Aly A I, Awad R and Rekaby M 2006 Magnetoresistance studies of Tl-1212 phase substituted by scandium *Supercond. Sci. Technol.* **19** 1104
[42] Mirzadeh M and Akhavan M 2005 Electrical and magnetic properties of Gd $(Ba_{2-x}La_x)Cu_3O_{7+\delta}$ *The European Physical Journal B-Condensed Matter and Complex Systems* **43** 305
[43] Marchetti M C 1991 Flux-line entanglement in high-T_c superconductors *Phys. Rev.* B **43** 8012
[44] Gaffney C, Petersen H and Bednar R 1993 Phase-slip analysis of the non-Ohmic transition in granular $YBa_2Cu_3O_{6.9}$ *Phys. Rev.* B **48** 3388
[45] Gamchi H S, Russell G J and Taylor K N R 1994 Resistive transition for $YBa_2Cu_3O_{7-\delta}$-Y_2BaCuO_5 composites: Influence of a magnetic field *Phys. Rev.* B **50** 12950
[46] Wright A C, Zhang K and Erbil A 1991 Dissipation mechanism in a high-T_c granular superconductor: applicability of a phase-slip model *Phys. Rev. B* **44** 863
[47] Mokhtari Z, Akhavan M and Khosroabadi H 2004 Thermally activated phase slip and variable range hopping in $Tm(Ba_{2-x}Pr_x)Cu_3O_{7+\delta}$ *Phys. Status Solidi* (C) **1** 1891
[48] Palstra T T M, Batlogg B, Schneemeyer L F and Waszczak J V 1988 Thermally activated dissipation in $Bi_{2.2}Sr_2Ca_{0.8}Cu_2O_{8+\delta}$ *Phys. Rev. Lett.* **61** 1662
[49] Iwasaki H, Kenmochi S, Tanigichi O and Kobayashi N 1994 Resistive superconducting transition of $Y_{1-x}Pr_xBa_2Cu_3O_y$ film in magnetic field *Physica B: Cond. Matt.* **194** 2117
[50] Savich S V, Kamchatnaya S N, Samoylov A V and Dobrovolskiy O 2017 Suppression of the order–disorder transition in Ti-doped YBaCuO compounds *J. Materials Science: Materials in Electronics* **28** 11415
[51] Hadi-Sichani B, Shakeripour H and Salamati H 2018 Magnetic field effect on the electrical resistivity of $Y_{1-x}Ni_xBa_2Cu_3O_{7-\delta}$ superconductor *Physica C: Superconductivity and its Applications* **549** 81
[52] Palstra T T M, Batlogg B, van Dover R B, Schneemeyer L F and Waszczak J V 1990 Dissipative flux motion in high-temperature superconductors *Phys. Rev.* B **41** 6621
[53] Abou-Aly A I, Awad R, Mahmoud S A and Ibrahim I H 2012 Magnetic transport properties in $GdBa_2Cu_{3-x}Ru_xO_{7-\delta}$ superconducting phase *J. Low Temp. Phys.* **167** 59
[54] Malik B A, Malik M A and Asokan K 2016 Magneto transport study of YBCO: Ag composites *Current Appl. Phys.* **16** 1270
[55] Hannachi E, Ben Salem M K, Slimani Y, Hamrita A, Zouaoui M, Ben Azzouz F and Ben Salem M 2013 Dissipation mechanisms in polycrystalline YBCO prepared by sintering of ball-milled precursor powder *Physica B: Cond. Matt.* **430** 52
[56] Wang Z H and Cao X W 1999 The effective activation energy U_e (T, H) in epitaxial $GdBa_2Cu_3O_{7-\delta}$ thin films *Solid State Commun.* **109** 709
[57] Aliabadi A, Akhavan-Farshchi Y and Akhavan M 2014 Flux dynamics in Y358 and Gd358 superconductors *J. Supercond. Nov. Magn.* **27** 741